# 'Natural' coordinates for analysis of the practical Stirling cycle

**A J Organ,** BSc, MA, PhD, CEng, MIMechE
Engineering Department, University of Cambridge

*The appropriate choice of coordinate system so simplifies basic cycle analysis that computation of the ideal particle trajectory diagram reduces to a straightforward graphical process. Ideal pressure, Reynolds number $N_{re}$, friction factor $C_f$ and heat-transfer parameters $N_{st}$ and $N_{pr}^{2/3}$ follow in function of location and crank angle via a few steps on the hand calculator. A thermodynamic design parameter is identified which has essentially the same numerical value for such diverse Stirling engines as Philips' MP1002CA, General Motors' GPU-3 and the turn-of-the-century Kyko hot-air engine.*

## NOTATION

| | |
|---|---|
| $A_{ref}$ | reference wetted area minus total gas circuit wetted area at crank angle for which cycle pressure is at reference value ($m^2$) |
| $A_{wfc}$ | total area of working fluid circuit wetted at reference conditions ($m^2$) |
| $A_x$ | cross-sectional area ($m^2$) |
| $C_f$ | friction factor; function of geometry and $N_{re}$, for example of $\P_v$, $N_{re}$ in the case of the wire mesh regenerator |
| $c_p$, $c_v$ | specific heat at constant pressure or volume (J/kg K) |
| $d_w$ | diameter of wire of regenerator gauze (m) |
| $F$ | wall friction effect per unit mass = $\frac{1}{2}u^2 C_f \operatorname{sign}(u)/r_h$ ($m/s^2$) |
| $g$ | mean mass velocity ($kg/m^2$ s) |
| $m$ | mesh number—number of wires/unit length (1/m) |
| $M$ | total mass of working fluid taking part in cycle (kg) |
| $n_{gauze}$ | total number of gauzes in regenerator stack |
| $n_s$ | cycles per second = $\omega/2\pi$ (1/s) |
| $N_B$ | Beale number = power/($n_s p_{ref} V_{ref}$) |
| $N_F$ | characteristic Fourier number = $\alpha_r/(n_s r^2)$ |
| $N_{MA}$ | characteristic Mach number = $n_s R_H/\sqrt{(RT_{ref})}$ |
| $N_{re}$ | local, instantaneous Reynolds number = $4\rho u r_h/\mu$ |
| $N_{RE}$ | characteristic Reynolds number = $N_{SG} N_{MA}^2$ |
| $N_{SG}$ | characteristic Stirling number = $p_{ref}/(n_s \mu_{ref})$ |
| $N_{st}$ | Stanton number = $h/(c_p g)$ |
| $N_T$ | characteristic temperature ratio = $T_e/T_{ref} = T_e/T_c$ |
| $N_{TCR}$ | characteristic thermal capacity ratio = $p_{ref}/(T_{ref} \rho_r c_r)$ |
| $p$ | absolute pressure (Pa) |
| $p_{ref}$ | reference pressure (Pa) |
| $q^*$ | heat-transfer rate per unit mass (W/kg) |
| $Q$ | heat quantity per cycle, for example $Q_E$ (J) |
| $r$ | offset of crank-pin (semi-stroke for no *désaxé* offset) (m) |
| $r_h$ | hydraulic radius (m) |
| $R$ | gas constant for specific gas (J/kg K) |
| $R_H$ | characteristic hydraulic radius of a Stirling cycle machine = $V_{ref}/A_{ref}$ (m) |
| $t$ | time (s) |
| $u$ | velocity (m/s) |
| $V_C$ | volume swept by compression space piston ($m^3$) |
| $V_E$ | volume swept by expansion space piston ($m^3$) |
| $V_d$ | dead (unswept) volume ($m^3$) |
| $V_{ref}$ | reference volume—gas circuit volume at $\phi$ for which $p = p_{ref}$ ($m^3$) |
| $V_{wfc}$ | volume of working fluid circuit wetted at reference conditions ($m^3$) |
| $W_{cycle}$ | indicated work per cycle (J) |
| $x$ | length coordinate (m) |
| $\alpha$ | volume phase angle in Schmidt analysis |
| $\alpha_x$ | area ratio = $A_x/A_{ref}$ |
| $\gamma$ | specific heat ratio = $c_p/c_v$ |
| $\zeta$ | specific cycle work = $W_{cycle}/(p_{ref} V_{ref})$ |
| $\eta$ | indicated thermal efficiency = $W_{cycle}/Q_E$ |
| $\kappa$ | ratio of swept volumes = $V_C/V_E$ |
| $\lambda$ | normalized length/distance = $l/L_{ref}$, $x/L_{ref}$ |
| $\lambda_h$ | normalized hydraulic radius = $r_h/L_{ref}$ |
| $\mu$ | coefficient of dynamic viscosity (Pa s) |
| $\mu_d$ | dead space ratio, for example $\mu_{dr} = V_{dr}/V_{ref}$ |
| $\mu_E$ | link between alternative bases for volume normalization = $V_E/V_{ref}$ |
| $\nu$ | independent variable—cumulative reduced dead space = $\int d\mu/\tau$ |
| $\mathbf{v}$ | total value of $\nu$ integrated between piston faces—function of $\phi$ |
| $\nu_D$, $\nu_D(N_T)$ | conventional dead space parameter = $\Sigma\mu_d/\tau$ (invariant with $\phi$) |
| $\rho$ | density ($kg/m^3$) |
| $\tau$ | dimensionless temperature = $T/T_{ref}$ |
| $\phi$ | crank angle (rad) |
| $\psi$ | dimensionless pressure = $p/p_{ref}$ |
| $\omega$ | angular frequency = $2\pi n_s$ (rad/s) |
| $\P_v$ | volumetric porosity $\approx 1 - \frac{1}{4}\pi m d_w$ for rectangular wire gauze |

### Subscripts

| | |
|---|---|
| c, C | compression space |

*The MS was received on 8 July 1992 and was accepted for publication on 30 October 1992.*

| | |
|---|---|
| d | dead space |
| dx | dead space in exchanger, for example, dxe = dead space in expansion exchanger |
| deriv | relating to derivative design |
| e, E | expansion space |
| proto | relating to prototype |
| r | regenerator |
| ref | reference value |
| w | wall |
| wfc | working fluid circuit |
| x | exchanger |

## 1 BACKGROUND

In 1947 deBrey *et al.* (**1**) drew attention to promising potential in the Stirling cycle machine, 'provided ... modern knowledge about heat transfer, flow resistance etc. is applied'. Half a century later, theoretical analysis does, indeed, aid practical development, but through the medium of exotic computer simulation manageable only by specialists. While there has been progress (**2–4**) in enfranchising thermodynamic tools, their potential for reducing the time and expense of initial design remains largely unexploited: despite arguments [for example reference (**5**)] to the contrary, an indefinite number of individuals and organizations competent and anxious to contribute to experimentation and development do *not*, for one reason or another, have the full benefit of the specialists' theoretical tools.

The point may be amplified by reference to the particle trajectory map. Of the various graphical descriptions of the practical cycle, this is arguably the single most important: it illustrates at a glance the fractions of working fluid (the 'inactive' elements) that fail to enter the exchanger system from the adjacent variable volume space; it predicts whether or not there will be parasitic slugs of gas oscillating in the exchangers without emerging from either end; it graphs the loci of latent discontinuities in temperature and turbulence level. Furthermore, it defines the coordinates of the Lagrange reference frame in which the conservation equations of one-dimensional flow with friction and heat transfer are most appropriately solved. Yet seldom is a particle trajectory map encountered as an adjunct to a practical design study, or to an account of a development programme or of an amateur design.

To the time of writing, construction of even the ideal, 'isothermal' map has called for lengthy algebraic manipulation (**6**, **7**). Digital computing facilities have been indispensable in converting that algebra to the familiar graphical form. With a simple transformation of length coordinate, on the other hand, construction of an accurate ideal trajectory map may now, if desired, be reduced to a matter of simple arithmetic and drafting. From the map in the new coordinates may be scaled pressure and the local, instantaneous Reynolds number, $N_{re}$, both in function of crank angle. From $N_{re}$, the local, instantaneous friction factor $C_f$ and the Stanton number $N_{st}$ follow in terms of cross-section geometry.

This is not to endorse the drafting option for all circumstances. On the contrary, those with preference for computing would be advised to continue. With the simpler formulation, however, they may do so more readily and with substantially reduced facilities: many programmable hand calculators should be able to handle the simplified task.

## 2 THE TEMPERATURE-DETERMINED CYCLE

The coordinate transformation is most readily illustrated in terms of the ideal, static 'isothermal' or temperature-determined cycle (Fig. 1). From the ideal gas equation the mass inventory is

$$M = \frac{p}{R} \times \left\{ \frac{V_e}{T_e} + \frac{V_{de}}{T_e} + V_{dr} \int \frac{d(x/L)}{T_e + (T_c - T_e)x/L} + \frac{V_{dc}}{T_c} + \frac{V_c}{T_c} \right\} \tag{1}$$

With $\mu$ to denote space normalized by $V_{ref}$,

$$M = \frac{pV_{ref}}{RT_{ref}} \left\{ \frac{\mu_e(\phi)}{N_T} + v_D(N_T) + \mu_c(\phi) \right\}$$

where $v_D(N_T)$ is the usual dead-space parameter (invariant with $\phi$) defined as

$$v_D(N_T) = \sum \frac{V_d/V_{ref}}{T/T_{ref}} = \frac{\mu_{de}}{N_T} + \frac{\mu_{dr} \ln(N_T)}{N_T - 1} + \mu_{dc} \tag{2}$$

Inverting the expression for $M$:

$$\frac{pV_{ref}}{MRT_{ref}} = \frac{1}{\mu_e(\phi)/N_T + v_D(N_T) + \mu_c(\phi)} \tag{3}$$

This equation holds at the value of $\phi$ for which $p$ has the reference value $p_{ref}$, for example $p_{max}$, $p_{min}$, $p_{mean}$:

$$\frac{p_{ref} V_{ref}}{MRT_{ref}} = \frac{1}{\mu_e(\phi_{ref})/N_T + v_D(N_T) + \mu_c(\phi_{ref})} \tag{4}$$

Combining equations (3) and (4),

$$\frac{p}{p_{ref}} = \frac{\mu_e(\phi_{ref})/N_T + v_D(N_T) + \mu_c(\phi_{ref})}{\mu_e(\phi)/N_T + v_D(N_T) + \mu_c(\phi)} = \psi \tag{5}$$

Equation (5) is valid where the variations of compression and expansion volumes are arbitrary functions of crank angle. To provide a specific instance, $V_E$ serves as $V_{ref}$, and volume variations are assumed to be simple harmonic with constant phase angle, $\alpha$, viz. $\mu_e(\phi) = \frac{1}{2}\{1 + \cos(\phi)\}$, $\mu_c(\phi) = \frac{1}{2}\kappa\{1 + \cos(\phi - \alpha)\}$:

$$\frac{p}{p_{ref}} = \frac{\frac{1}{2}\{1 + \cos(\phi_{ref})\}/N_T + v_D(N_T) + \frac{1}{2}\kappa\{1 + \cos(\phi_{ref} - \alpha)\}}{\frac{1}{2}\{1 + \cos(\phi)\}/N_T + v_D(N_T) + \frac{1}{2}\kappa\{1 + \cos(\phi - \alpha)\}} \tag{6}$$

The numerator of equation (6) is a constant.

A new variable, $v$, is now defined as $v = \int d\mu/\tau$. The integral is reckoned from the piston face (Fig. 1) rightwards to a point, $x$, in the gas circuit of current interest. The new independent variable might be called the *cumulative reduced volume*, since it is evaluated in the same way as $v_D$. With $\mathbf{v}$ to represent $v$ integrated over the entire distance between piston faces it is clear that $\mathbf{v}_{ref}$ is

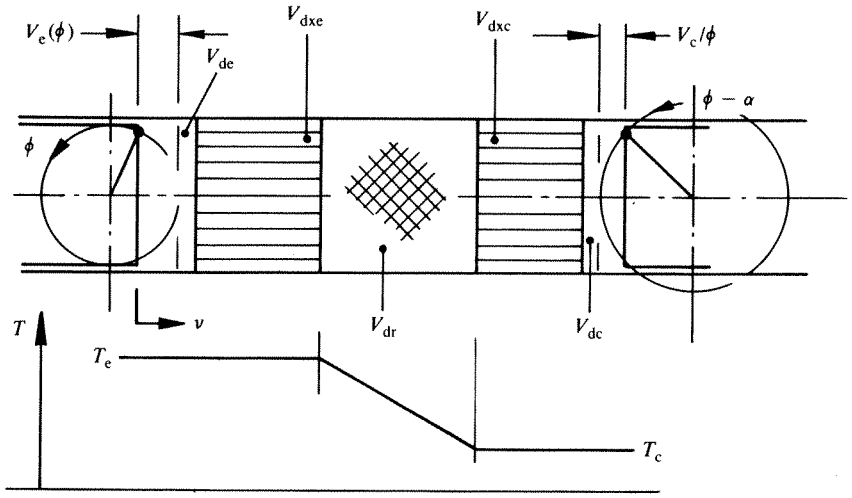


**Fig. 1** Equivalent Stirling machine gas circuit

constant:

$$\frac{p}{p_{ref}} = \psi = \frac{\mathbf{v}_{ref}}{\mathbf{v}} \tag{7}$$

In symbolic form at least, equation (7) is a great simplification over the source equation (6).

In equation (1) *all* dead space at $T_e$ was conveniently represented by $V_{de}$. The fluid particle trajectory map is more useful if it indicates the distinction between $V_{de}$ (unswept in the variable-volume space) and $V_{dxe}$ (dead volume internal to the fixed-volume exchanger). From this point, the distinction will be made.

What is meant by an increment, d$v$, in $v$ is an increment in the $x$ direction encompassing a dimensionless mass increment in the ratio $dm/M = dv/\mathbf{v}$. In other words, in a gas circuit whose linear distances are described in terms of the variable $v$, equal subdivisions contain mass elements of equal magnitude. Put another way, individual contributions $v_i$ to overall reduced length *have the same numerical values as their respective numerical contributions to the dead-space parameter* $v_D$.

Looking ahead, construction of the fluid particle displacement map will involve simply drawing out the gas circuit, including piston positions, in $\phi$–$v$ coordinates and subdividing the distance between the piston faces at any given crank angle into equal increments. Joining up the subdivisions will define particle trajectories in the new coordinates. These are readily transformed back to the more usual $\phi$–$x$ system. The combined process is simpler than computing from the outset in $\phi$–$x$ coordinates and, indeed, may be accomplished on the drafting machine.

## 3 THE IDEAL PARTICLE TRAJECTORY MAP

Figure 2 shows the initial stages of the construction of a particle trajectory map in 'natural' coordinates. A specific Stirling engine is represented, namely the Philips MP1002CA (Table 1). The coaxial layout is pretransformed into the opposed-piston equivalent. This involves conversion of the *actual* piston phase angle $\beta$ and piston displacement ratio $\lambda$ respectively to the volume phase angle $\alpha$ and swept volume ratio $\kappa$ [via, for example, the relationships given in reference (2) or (3)].

Individual steps in $v$ are now calculated as $\mu_i/\tau_i = (V_i/V_{ref})/(T_i/T_{ref})$ for volume $i$. For example, the reduced length contribution of the expansion cylinder *total displacement* is $(V_E/V_{ref})/N_T = \mu_E/N_T$. Where $V_E$ is the choice for $V_{ref}$, this reduces to the particularly simple expression $1/N_T$. The instantaneous expansion cylinder

**Table 1** Numerical values of dimensionless groups at rated conditions for the Philips MP1002CA air engine. A set of numerical values for the dimensionless variables tabulated amounts to a complete thermodynamic description of the equivalent machine

| Symbol | Definition | Rated value |
|---|---|---|
| Rated working fluid | | Air |
| $n_s$ | Revolutions per second | 25 (1/s) |
| $p_{ref}$ | Reference charge pressure | 15.0E + 05 (Pa) |
| $T_{ref}$ | Reference (ambient) temperature | 333 (60°C) (K) |
| $V_{wfc}$ | (See Notation) | 0.12E-03 ($m^3$) |
| $V_E$ | Swept volume by expansion space | 0.062E–03 ($m^3$) |
| $A_{ref} = A_{wfc}$ | (See Notation) | 0.55 ($m^2$) |
| $\kappa$ | Volume ratio $V_C/V_E$ | 1.031 |
| $\alpha$ | Equivalent phase angle, rad (deg) | 2.1 (121°) |
| $R_H$ | $V_{wfc}/\Sigma A_w$ | 0.216E-03 (m) |
| $\P_v$ | Volume porosity regenerator | 0.80 |
| $\zeta_{ind}$ | $P_{ind}/(n_s p_{ref} V_E)$ | 0.13 |
| $\mu_E$ | $V_E/V_{wfc}$ | 0.514 |
| $R_H/r$ | Compactness ratio | 0.0173 |
| $\mu_{de}$ | $V_{de}/V_{ref}(V_{ref} = V_E)$ | 0.123 |
| $\mu_{dxe}$ | $V_{dxe}/V_{ref}$ | 0.092 |
| $\mu_{dr}$ | $V_{dr}/V_{ref}$ | 0.313 |
| $\mu_{dxc}$ | $V_{dxc}/V_{ref}$ | 0.092 |
| $\mu_{dc}$ | $V_{dc}/V_{ref}$ | 0.146 |
| $\alpha_{xxe}$ | $A_{xxe}/A_{ref}$ | 0.37E-03 |
| $\{\alpha_{xr}$ | $A_{xr}/A_{ref}$ | 1.302E-03} |
| $\alpha_{xxc}$ | $A_{xxc}/A_{ref}$ | 0.37E-03 |
| $\lambda_{hxe}$ | $r_{hxe}/L_{ref}(L_{ref} = r)$ | 0.0137 |
| $\lambda_{hr}$ | $r_{hr}/L_{ref}$ | 0.0032 |
| $\lambda_{hxc}$ | $r_{hxc}/L_{ref}$ | 0.0137 |
| $N_T$ | $T_e/T_c$ | 2.65 ($T_e$ = 333 K) |
| $\gamma$ | $c_p/c_v$ | 1.4 |
| $N_{MA}$ | $n_s r/\sqrt{(RT_{ref})}$ | 1.01E-03 |
| $\{N_{PR}$ | $\mu c_p/k$ | $\approx$1.0} |
| $N_{SG}$ | $p_{ref}/(n_s \mu)$ | 3.30E + 09 |
| $N_{TCR}$ | $p_{ref}/(T_{ref} \rho_r c_r)$ | 0.0011 |
| $N_F$ | $\alpha_r/(n_s r^2)$ | 0.0013 |

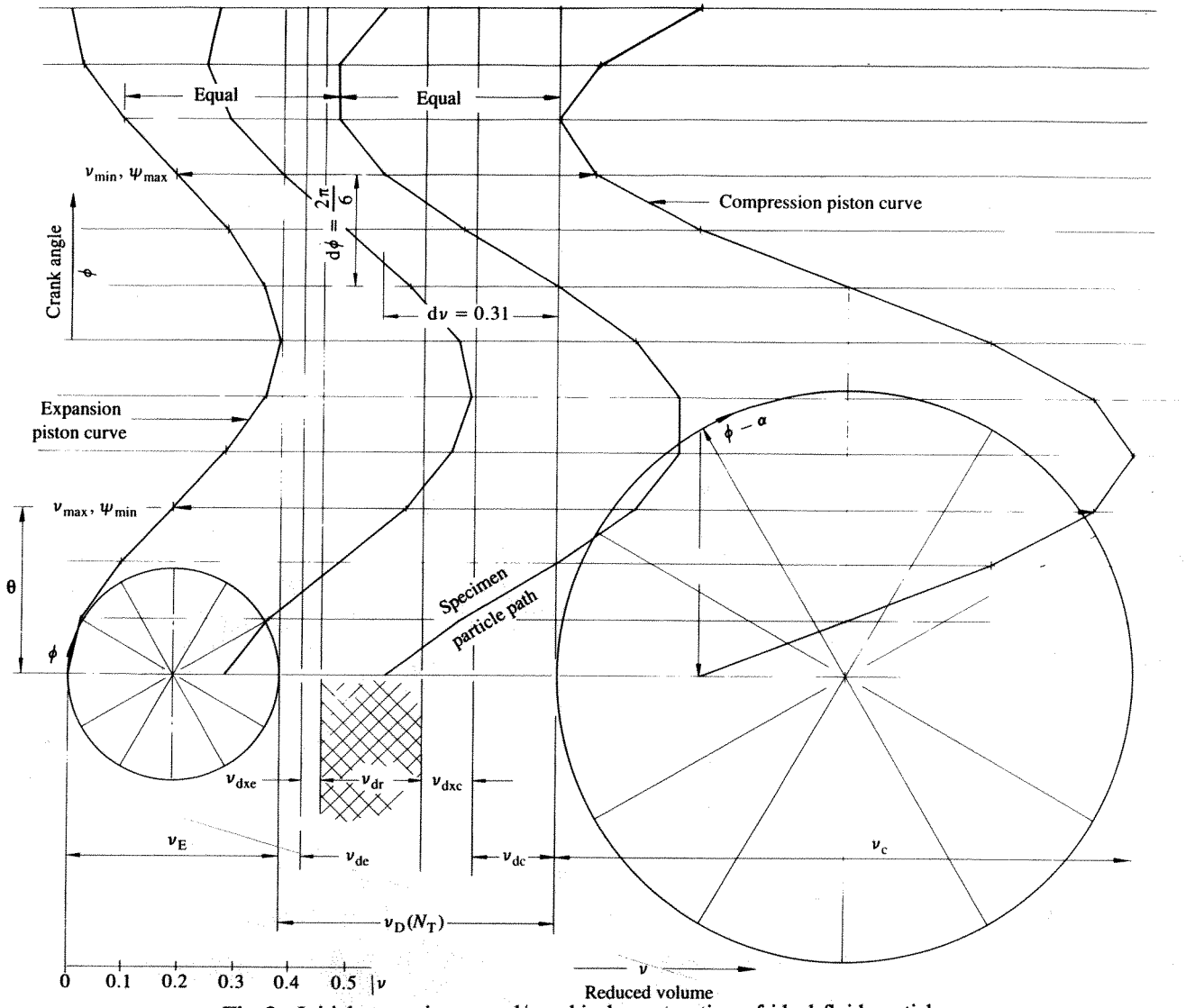


**Fig. 2** Initial stages in manual/graphical construction of ideal fluid particle trajectory map. Parameters are for the Philips MP1002CA air engine

*volume* contributes $\mu_e(\phi)/N_T$, the reduced length of the compression exchanger, for example, is $\mu_{dxc} = V_{dxc}/V_{ref}$ and the reduced length of the regenerator is $\mu_{dr} \ln(N_T)/(N_T - 1)$.

Expansion and compression piston face motion is generated by projecting from equal subdivisions of circular arcs of radius $\frac{1}{2}\nu_E$ and $\frac{1}{2}\nu_C$ (that is $\frac{1}{2}\mu_E/N_T$ and $\frac{1}{2}\mu_C = \frac{1}{2}\kappa N_T \nu_E$ respectively). Dividing the horizontal linear distance between face positions into $n$ equal increments and repeating for a sequence of crank angles $\phi$, yields traces of the motions of $n$ particles as a function of $\phi$.

Converting back to 'real' coordinates involves first of all laying out the gas circuit and piston motions (that is the piston motions of the opposed-piston machine). The transference of particle positions is carried out by considering first of all the uniform-temperature spaces: a particle in the transformed plane that lies, say, at the mid-point of the expansion exchanger also lies at the mid-point of the *actual* exchanger. Other locations are pro-rated. A particle whose location from, say, the left-hand end of the regenerator measured in 'natural' coordinates is $\nu'$ (from the regenerator inlet) relocates at point $\lambda'$ in 'real' coordinates, where $\lambda'$ is the distance from the regenerator inlet as a fraction of total (true) regenerator length:

$$\lambda' = \frac{\exp\{(1 - N_T)\nu'/\mu_{dr}\} - 1}{1/N_T - 1} \tag{8}$$

Trajectory plots produced on this two-step principle, whether manually or by computer, involve a fraction of the work of previous methods [for example those of references (6) and (7)] carried out in traditional coordinates. For example, a computer implementation in FORTRAN 77, providing a choice of volume functions, scaling and preparation for plotting, runs to a mere 68 executable assignments. A general-purpose subroutine for conversion back to 'real' coordinates adds only another 36 assignments. On this basis, an equivalent program (probably in a lower level language) is a realistic proposition for the programmable hand calculator.

The trajectory map yields ideal pressure as a function of crank angle directly and ideal indicator diagrams indirectly: pressure (absolute or normalized) is a minimum at the value of $\phi$ for which $\nu$ (reduced total distance between the piston faces) is a maximum; minimum pressure occurs where $\nu$ is a minimum. These

values are readily determined by inspection. If $p_{ref}$ has been chosen to be $p_{min}$, then $v$ on the map = unity at the $p_{min}$ point and all other $v$ values are less than unity. If $p_{max}$ has been chosen for $p_{ref}$, then $v$ is unity again at the $p_{max}$ point and all other $v$ values are greater than unity. Pressures intermediate to the extremes may be picked off at regular intervals in terms of the ratio $p/p_{ref} = v_{ref}/v$. Corresponding to each $p/p_{ref}$ may be picked off a $V/V_{ref}$ for both of the two working spaces. Dimensionless indicator diagrams follow. Pressure traces and indicator diagrams are not illustrated; construction is trivial—by contrast with the tedious numerical substitutions required when working from formulae [equation (5) or equivalent].

## 4 IMPLICATIONS FOR UNDERSTANDING THE IDEAL 'STATIC' CYCLE

Figure 3a and b is for the MP1002CA engine at rated conditions (Table 1). In 'traditional' presentation, path lines denoting the boundaries of equal subdivisions of working fluid mass are packed more closely at the compression (low-temperature) end due to the higher density. The bias of working fluid mass to the cold end is highlighted by use of 'natural' coordinates (Fig. 3a) with its equal subdivisions. The ideal, 'textbook' (3) cycle calls for the condition:

$$\frac{Q_E}{T_E} = \frac{Q_C}{T_C} = \text{constant} = MR \ln(\text{expansion ratio}) \qquad (9)$$

in other words, for a greater heat load at the expansion end. It might be supposed from this that the appropriate starting point for the design ought actually to be the *opposite* bias of working fluid mass.

In searching for an explanation it might first be supposed that the MP1002CA is not an optimum design—even by the idealized criteria of the 'isothermal' analysis. On the evidence of heat exchanger channel proportions alone it almost certainly is not: expansion and compression exchangers are geometrically identical—an unlikely choice for dealing with different heat rates under different thermodynamic conditions.

On the other hand, the dead-space parameter $v_D$ (based on $V_{ref} = V_E$) is 0.49 for the MP1002CA. The typical isothermal optimization chart [for example the selection of reference (3)] indicates optimum $\kappa$ of the order of unity ($V_C \approx V_E$) at this $v_d$ and rated $N_T$. This is essentially the value actually embodied in the MP1002CA (Table 1) and therefore the one giving rise to the unexpected working fluid distribution. The observation is no support for the earlier inference.

The explanation lies in reconsideration of the right-hand side of equation (9), which presupposes that compression takes place with the entire working fluid mass, $M$, in the compression space and expansion with the entire mass in the expansion space. For equation (9), the volume ratio is unity by definition (because compression and expansion ratios are the same) and the density of fluid particle paths is symmetrical at either end of the machine. Takase (8) extended the range of his isothermal optimization chart for $\zeta_{max}$ ($= W_{cyc}/p_{max} V_{ref}$) of the opposed-piston machine to include $v_D(N_T) = 0$. Figure 4 is a reproduction of the relevant part of Takase's chart $\kappa$ showing that $\kappa \approx 1/N_T$ over a wide range of $N_T$ provided $v_D = 0$. When the 'natural' coordinate map is redrawn for the case $v_d = 0$, as is done in Fig. 5, mass distribution is symmetrical, as required by equation (9).

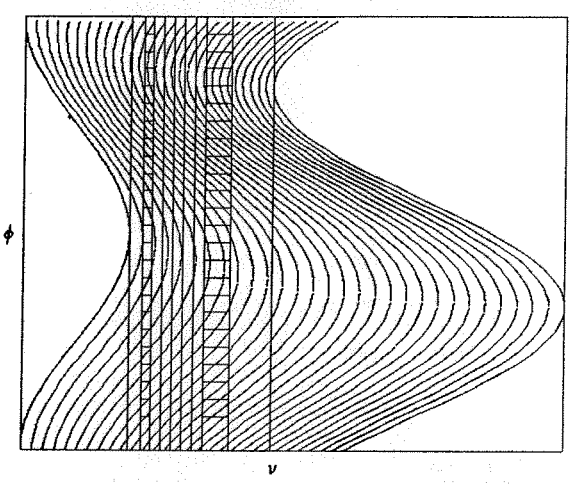


(a) Representative ideal fluid particle trajectory map in 'natural' coordinates

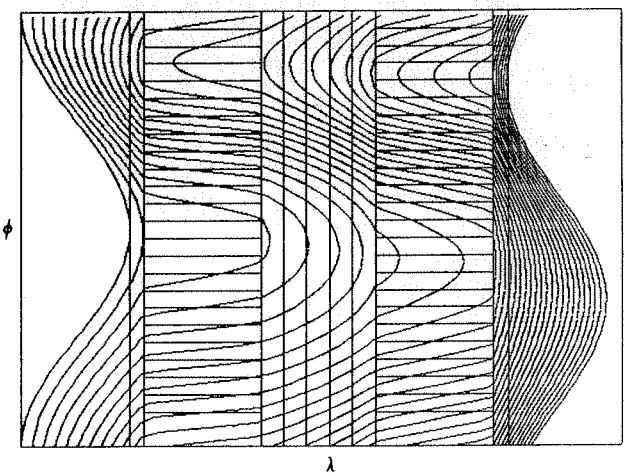


(b) Ideal map transformed from 'natural' to conventional coordinates

**Fig. 3** Comparison of ideal fluid particle trajectory maps in 'natural' and conventional coordinates, showing particularly how 'natural' coordinates emphasize bias of working fluid mass towards the compression end for the MP1002CA

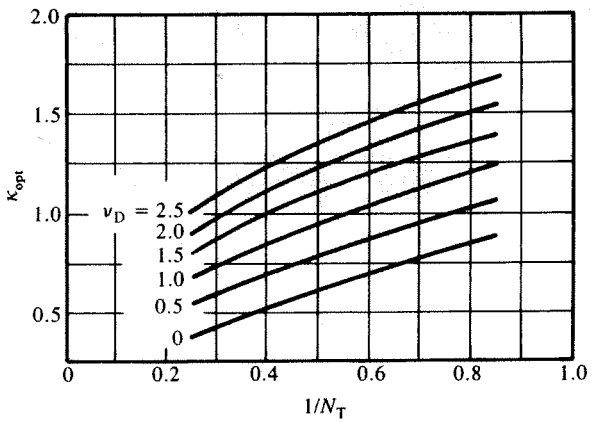


**Fig. 4** Takase's isothermal optimization curves include the extreme case $v_D = 0$, permitting interpretation of equation (9) in terms of the Schmidt model. $\kappa_{opt}$ for this hypothetical case (zero dead volume) $\approx$ constant/$N_T$

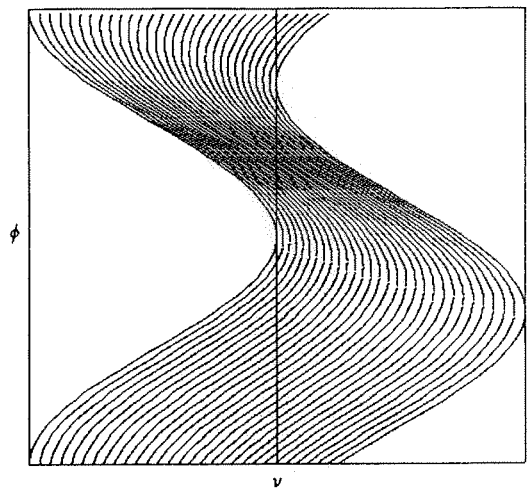


**Fig. 5** Map redrawn in 'natural' coordinates using the value of $\kappa$ for which specific cycle work $\zeta$ is optimum in the hypothetical case of zero unswept volume. The distribution of mass between the expansion and compression ends is now symmetrical

The asymmetry of the ideal 'static' cycle for $v_d > 0$ may reflect the fact that, with these realistic values of $v_D$, compression and expansion no longer follow the law for the uniform, isothermal mass (3), that is $pV \neq$ constant. On the other hand, a simple criterion for desirable mass distribution does not emerge. The only firm conclusion to be drawn is that intuition is a treacherous tool for investigation of the innocent Stirling cycle.

## 5 IMPLICATIONS FOR PRACTICAL DESIGN

There are two extreme approaches to mechanical design—*scaling* from precedents, and first-principles *analysis* applied to elemental sub-systems. Comprehensively carried out, scaling provides a guarantee of performance, since the end product is dynamically similar to its prototype, and so has no option but to perform to scale. On the other hand, such dynamic similarity is possible only on the basis of strict geometric similarity (9). That exact geometric replicas are seldom desired is surprising until it is noted (a) that strict geometric scaling stifles innovation and (b) that when dynamically scaled (*dimensionless*) performance is interpreted in terms of its *absolute* parameters (revolutions per minute etc.) the latter may be unacceptable.

Most practical design is a balance between the two extreme approaches. In the case of Stirling machines, the tools for formal scaling are of relatively recent origin (2–4). They include the dimensionless parameters tabulated in the Appendix. These are not arbitrary combinations of the absolute variables: each has a readily appreciated physical significance in the context of the Stirling gas circuit. The Appendix amplifies.

To keep the example manageable, *internal* scaling only will be applied. This supposes that the internal walls of the heat exchangers can be maintained at rated values for all choices of the variables—in other words, heat-transfer processes between combustion products and the expansion exchanger inner surface and between the compression exchanger inner surface and coolant are not considered. These processes may be taken into account by a straightforward extension of the method.

It is shown elsewhere (2–4) that performance scaling between geometrically similar machines may be achieved by serial substitution of the dimensionless groups of the Appendix—either by hand calculator or via pre-printed nomograms. Thus, the trajectory map is not strictly necessary in the example chosen. However, its use will provide independent support for the scaling method and illustrate the computational processes required when deviating from geometric similarity.

The gas circuit to be designed will be a scaled down (half-cubic displacement) MP1002CA with hydrogen (diatomic) as the working fluid and operating at the same temperature limits as the original (Table 1). By definition, the specific indicated cycle work $\zeta = W_{cyc}/(p_{ref} V_{ref})$ and the indicated thermal efficiency $\eta$ will remain the same, but the power output will be different because of the new rotational speed $n_s$ and reference pressure (to be determined as part of the scaling process). Linear dimensions will be reduced in the ratio $\sqrt[3]{0.5} \approx 0.8$.

The ideal particle trajectory map is independent of angular speed, so the map already plotted (Fig. 2) applies. The map taking account of friction and heat transfer [for example as discussed in reference (3) for the MP1002CA] does not, except by coincidence, correspond exactly with the ideal counterpart. On the other hand, maps for dynamically similar 'real' machines are identical. On this basis the ideal map is taken as an *approximation* to the map for the MP1002CA and for any machine scaled from it.

Local, instantaneous Reynolds and Mach numbers, $N_{re}$ and $N_{ma}$, may be expressed in terms of the dimensionless parameters of the gas circuit. Both embody a value of local, instantaneous particle velocity, $u = \mathrm{d}x/\mathrm{d}t$. With $\mathrm{d}\phi = \omega\, \mathrm{d}t = 2\pi n_s\, \mathrm{d}t$ and taking into account the definition of $v$,

$$u = 2\pi n_s r \frac{\mathrm{d}v}{\mathrm{d}\phi} \frac{\tau}{\alpha_x} \frac{R_H}{r} \tag{10}$$

$N_{re}(x, t) = 4r_h \rho u/\mu$, in which $r_h$ is a function of location, $x$, and both $\rho$ and $u$ are functions of both $x$ and $t$. Strictly, $\mu$ (coefficient of dynamic viscosity) is a function of $T(x, t)$, and therefore a function of both $x$ and $t$. To a close approximation, $T(x, t) \approx T_w(x)$, leaving $\mu = \mu(x)$. It is a simple matter (and, indeed, an essential part of the scaling process) to take account of the dependence on location $x$, but for compactness of presentation, the treatment will proceed on the basis of $\mu$ invariant at the reference (ambient) value.

Taking account of the definitions of the characteristic parameters $N_{SG}$ and $N_{MA}$:

$$N_{re}(v, \phi) = 8\pi N_{SG} N_{MA}^2 \frac{\lambda_h}{\alpha_x} \frac{R_H}{r} \psi \frac{\mathrm{d}v}{\mathrm{d}\phi} \mu_E \tag{11}$$

Despite being expressed as a function of $v$ and $\phi$, $N_{re}$ here has the numerical value that applies at rated conditions in the functioning (ideal) machine. A value for the $\mathrm{d}v/\mathrm{d}\phi$ term comes straight from the trajectory map as the measured value of the ratio $\Delta v$ to $\Delta\phi$ (in the units of the respective axes). $N_{SG}$ and $N_{MA}$ have the same numerical value by definition between prototype and derivative. The length scales $\lambda_h$, $R_H/r$ and normalized area $\alpha_x$ are also the same between the prototype and linearly scaled derivative. Therefore $N_{re}$ *is the same*

*between the two machines for all x and t.* It follows immediately that the friction factor $C_f = C_f$ (geometry, $N_{re}$)† is the same at all $x$ and $t$.

In Fig. 2, $dv/d\phi$ is constructed in the vicinity of maximum pressure as $0.21/(2\pi/6) \approx 0.20$. The value applies at the compression end of the regenerator and at the regenerator end of the compression exchanger, giving, from equation (11), $N_{re} \approx 370$ (peak) for the former location and 0.5E + 04 for the latter. The peak $dv/d\phi$ on the left-to-right pass slightly exceeds the specimen value, but $\psi$—and thus density—is lower, so the $N_{RE}$ calculated are close to respective maxima for the cycle at rated conditions.

The local, instantaneous Mach number, $N_{ma}(x, t)$, is defined as $u/\sqrt{(\gamma RT)}$. Inserting equation (10) for $u$:

$$N_{ma}(v, \phi) = \frac{2\pi}{\alpha_x}\frac{R_H}{r}\sqrt{\left(\frac{\tau}{\gamma}\right)}N_{MA}\frac{dv}{d\phi} \tag{12}$$

At corresponding locations and crank angles the $dv/d\phi$ are the same between the prototype and derivative design, as are the length and area ratios; $\gamma$ is the same for $H_2$ as for air. The $\tau(x, t)$ are nominally the same, because of the proximity of $T(x, t)$ to $T_w(x)$. It can, however, be shown that they are *identical* for all $x$, $t$, as follows.

The energy equation in Lagrange coordinates (for present purposes the choice of coordinates is immaterial, but the Lagrange form is simplest) is

$$c_p\frac{DT}{dt} - \frac{RT}{p}\frac{Dp}{dt} = q^* + uF \tag{13}$$

In equation (13), $q^* = h(T_w - T)/(\rho r_h)$ and $F = \frac{1}{2}u^2C_f\,\text{sign}(u)/r_h$. Substituting these definitions together with equation (10) for $u$ and normalizing:

$$-(\gamma - 1)\frac{1}{\gamma\psi}\frac{D\psi}{d\phi} + \frac{1}{\tau}\frac{D\tau}{d\phi} = N_{st}\left[\frac{\{\tau_w(\lambda) - \tau\}}{\alpha_x\lambda_h}\frac{dv}{d\phi}\frac{R_H}{r} + 2\pi^2\frac{\gamma - 1}{\gamma\lambda_h}N_{MA}^2\frac{R_H^3}{r^3}\frac{\tau^2}{\alpha_x^3}\left(\frac{C_f}{N_{st}}\right)\left|\frac{dy}{d\phi}\right|^3\right] \tag{14}$$

Given that $N_{re}(v, \phi)$ is the same for all $v$, $\phi$, then $N_{st}(v, \phi)$ is also the same for all $v$, $\phi$, and so, from previous reasoning, is the ratio $C_f/N_{st}$. Equation (14) now says a great deal about the Stirling machine gas processes:

1. The final term in the equation defines local, instantaneous dissipation, and is always positive. This is assured, despite dispensing with the $u/|u|$ term, by transferring the exponent (3) of $u$ to the modulus of $dv/d\phi$.
2. $\tau$ is the sole unknown in equation (14), all parameters and constants being identical between prototype and derivative design. Without solving the equation it can therefore be said that $\tau(v, \phi) = T(v, \phi)/T_{ref}$ is identical between the two cases. This permits the conclusion that the $N_{ma}(v, \phi)$ are also the same, and will permit proof (see below) that fractional pressure gradients $\Delta p(v, \phi)/p(v, \phi)$ are the same for all $v$, $\phi$.
3. The right-hand side contains the ratio $C_f/N_{st}$. This reflects an invaluable contribution to Stirling machine design expounded by Creswick (**11**) but not, as far as is known, followed up. Creswick observed that, for a wide range of heat-transfer surface geometries, correlations between $N_{st}N_{pr}^{2/3}$ and $N_{re}$ and between $C_f$ and $N_{re}$ are essentially parallel in log–log format, giving, as an approximation, $N_{st}N_{pr}^{2/3}/C_f \approx$ constant or, since $N_{pr}$ tends to have a constant value close to unity, $N_{st}/C_f \approx$ constant. If it were thought suitable to digress from the rectangular slotted channel arrangement of the heater and cooler of the MP1002CA design, Creswick's observation suggests the use of the cross-section, giving the largest ratio of $N_{st}N_{pr}^{2/3}/C_f$.

Having established the equivalence of the $N_{ma}$ it is possible to turn to the matter of pressure gradients. The well-known expression for the steady flow pressure drop is

$$\frac{dp}{dx} = -\frac{1}{2}\rho u^2 C_f\frac{\text{sign}(u)}{r_h} \tag{15}$$

Substituting for $\rho = p/(RT)$ from the ideal gas equation, and recalling the definition of $N_{MA}$,

$$\frac{|\Delta p|}{p} = \frac{1}{2}\gamma N_{MA}^2 C_f\left(\frac{\Delta x}{r_h}\right)\frac{\text{sign}(u)}{\tau} \tag{16}$$

Equation (16) confirms that, over any given fractional length of heat exchanger, $\Delta x/r$, the fractional pressure gradient, $\Delta p/p$ (or $\Delta p/p_{ref}$), is the same for all $\phi$ between dynamically similar machines.

It remains to examine the thermal performance of the regenerator. The geometric similarity condition means that, in addition to the requirement for $\P_v$, $\lambda_{hr}$ to have the same value between the prototype and derivative design, the method of construction must be identical. The MP1002CA has a regenerator filament wound *in situ* from crimped stainless steel wire. The rigorously scaled regenerator must be made in the same fashion using the same number of turns and the same number of layers. Common sense suggests that the strict geometric requirement might be relaxed in favour of an alternative construction provided it yields the $\P_v$ and $\lambda_h$ of the MP1002CA regenerator.

The thermal response of the geometrically similar regenerator is scaled by use of the parameters $N_{TCR}$ and $N_F$—both of which are explained in the Appendix. To proceed, it is necessary to know the $p_{ref}$ and $n_s$ of the scaled design. The relative $n_s$ are obtained by equating the $N_{MA}$, leading to $(n_s)_{deriv}/(n_s)_{proto} = (r_{proto}/r_{deriv})\sqrt{(R_{deriv}/R_{proto})} = 4.74$; in other words, for dynamic similarity the crankshaft must rotate at $4.74 \times 1500$ r/min or about 7000 r/min. There is nothing exceptional about this figure in the context of other prime movers of the size proposed, namely of $60 \times 0.5 = 30$ cm$^3$. However, the high speed *at the original value of* $\zeta$ already threatens high heat flux rates which must be achieved by conduction through cylinder walls if MP1002CA geometry is to be retained; this may not be achievable.

The new $p_{ref}$ follows by equating the $N_{SG}$, which results in $(p_{ref})_{deriv} = 14 \times 2.37 = 33.2$ bar. Presupposing feasible regenerator design, projected power (from the definition of $\zeta$) is that of the MP1002CA pro-rated

† It is demonstrated elsewhere (**10**) that $C_f$ is strictly also a function of Mach number, $N_{ma}$. Since it is about to be shown that $N_{ma}$ is the same for all $x$ and $t$ between the prototype and derivative, there is no compromise.

by $(p_{ref} V_{ref} n_s)_{deriv}/(p_{ref} V_{ref} n_s)_{proto}$, that is an increase in the ratio 5.36. The proposed reduction in cylinder diameter is only 20 per cent. With pressure more than doubled wall thickness must be doubled. The possibility of achieving the fivefold increase in the heat rate through twice the original wall thickness and through a free-flow area $0.8^2$ of the original suggests a wall temperature gradient increased in the ratio $5 \times 2/0.8^2$, that is sixteenfold if the same materials are used. The prospect is unattractive, and it is already clear that *overall* dynamic similarity cannot be achieved unless some means can be identified of transferring flow to passages having the original geometry but in the form of separate channels external to the main pressure vessel.

At this stage either a failed undertaking can be bemoaned or a technique that has pre-empted wasted design—and possibly manufacturing—effort can be celebrated. Either way, it will be worth concluding the calculations as an illustration of the method.

The condition for assuring similarity of heat flows within individual wires of the regenerator is: $(N_F)_{deriv} = (N_F)_{proto}$, requiring $(\alpha_r)_{deriv} = (\alpha_r)_{MP1002CA}(r^2 n_s)_{deriv}/(r^2 n_s)_{MP1002CA}$, where $\alpha$ is thermal diffusivity. Inserting numerical values, $(\alpha_r)_{deriv} = 3.2(\alpha_r)_{MP1002CA}$. Stainless steel (the material of the MP1002CA) has $\alpha$ of the order of 4E-06 m/s. Copper, for example, has 105E-06, commercial bronze 56E-06 and aluminium bronze 64E-06 m/s, so the required thermal property *per se* is realizable. The material is going to have to be acquired in wire form to 0.8 of the diameter of the original stainless steel, and be sufficiently robust to permit crimping and filament winding.

The $N_F$ condition must be complemented by that for comparable thermal capacity ratios. The condition $(N_{TCR})_{deriv} = (N_{TCR})_{proto}$ reduces for the present case ($T_{ref}$ common to both designs) to $(\rho_r c_r)_{deriv} = (\rho_r c_r)_{MP1002CA}(p_{deriv}/p_{MP1002CA})$—in other words, a factor of $33/14 = 2.36$ increase in $\rho_r c_r$ of the new design. This might be thought modest in view of the greater specific heat of the proposed $H_2$ over the original air, until it is noted that, at common $T_{ref}$, total $H_2$ mass is less than that of air in the ratio $p_{H_2} R_{air}/(p_{air} R_{H_2})$. Values of $\rho_r$ and $c_r$ are available for candidate materials in Table AXII.5.2 of reference (**3**). None of the usual materials affords the desired increase of 2.36 in the product.

An engine constructed to the proposed geometry and charged with hydrogen to the new pressure would almost certainly function in some fashion. Indeed, it might conceivably outperform its prototype in the sense of having greater $\zeta$ and $\eta$. It will not, except by coincidence, perform as a scaled MP1002CA. The present method does not predict performance that is not to scale.

## 6 RELEVANCE BEYOND GEOMETRIC SIMILARITY

The Stirling cycle unit comprises two variable-volume spaces, two heat exchangers, a regenerator and means of maintaining the exchangers at $T_e$ and $T_c$. There are no valves. Working fluid behaviour is effectively independent of the nature of heat source and sink. A simpler concept for converting heat to work would be difficult to imagine, yet a straightforward guide to the relationship between performance requirement, operating parameters (revolution per minute, charge pressure, working fluid) and gas circuit geometry has never been explicitly proposed. [The 'Beale' number (**3**) is a performance 'upper bound' rather than a design guideline.]

The challenge reduces to specifying the relationship between the heat-transfer capability of the gas circuit and the heat capacity requirement of the working fluid. The appropriate symbolic form was anticipated decades ago by Finkelstein (**12**) in the dimensionless heat-transfer parameter of his 'generalized thermodynamic analysis'. For a variable-volume working space this may be restated as $N_{ST} = hA_w/(n_s c_p M)$. Clearly a form of Stanton number, $N_{ST}$ is the ratio of heat rate available by convection to rate of heat take-up by a mass rate of working fluid proportional to $n_s M$. $N_{ST}$ comes close to being the philosopher's stone of Stirling machine design. It falls short to the extent that $h$ is not specified until geometry and operating conditions are set, and so is not yet in a usable form.

Between dynamically similar machines, *all* $N_{st}$ $(=h/c_p g)$ at all locations are proportional to $N_{ST}$ for all $\phi$, and such local $N_{st}$ are also a statement of the essential relationship between the local, instantaneous rate of heat supplied by convection to the rate of working fluid take-up. For a given flow passage geometry, $N_{st} = N_{st}(N_{re} N_{pr}^{2/3})$ and, within limits close enough for present purposes, correlations for smooth flow passages based on $r_h$ are essentially common, as are those for flow passages interrupted in the fashion of wire screens. It has already been shown that $N_{re}(x, t)$ are identical at corresponding $x$ and $t$ in dynamically similar machines. Expressing $N_{re}$ in terms of the defining dimensionless groups will therefore give the condition for similar $N_{ST}$.

This, of course, has already been done, leading to equation (11), where instantaneous $N_{re}$ is seen to be a function of the principal characteristic parameters and of two quantities varying with $\phi$. There is no loss of generality in using, say, *peak* $N_{re}$ to characterize *all* $N_{re}$, so for a selected location within the machine equation (11) may be rewritten as

$$N_{re}(v) = 8\pi N_{RE} \frac{\lambda_h}{\alpha_x} \frac{R_H}{r} \psi_{max} \left(\frac{dv}{d\phi}\right)_{max} \tag{17}$$

In equation (17), $N_{RE} = N_{SG} N_{MA}^2$, as defined elsewhere. While there may be all the difference in the world between $p_{max}$ and $u_{max}$ of different designs, the *dimensionless* forms, $\psi_{max}$ and $(dv/d\phi)_{max}$ are likely to vary little. The term $8\pi$ is of no consequence, so equation (17) simplifies to

$$N_{re}(v) \propto N_{RE} \frac{\lambda_h}{\alpha_x} \frac{R_H}{r} \tag{18}$$

The strict criterion for dynamic similarity is for *all* individual terms of equation (17) to have the same numerical values between the prototype and derivative design. However, it is now clear that *the* $N_{re}$ *and therefore the* $N_{st}$ *will be nominally the same if the net numerical value of the right-hand side of equation (18) is the same in both cases.*

Equation (18) is the working equivalent of Finkelstein's statement of thermodynamic similarity. It has focused on the paramount matter of heat transfer to the apparent exclusion of flow friction. On the other hand, for a given geometry, $C_f = C_f(N_{RE})$. Machines with a comparable equation (18) are therefore already well on

the way to having similar dimensionless pressure profiles.

Equation (18) deals with the relationship between working fluid properties, operating conditions and gas circuit *geometry*. It says nothing about the regenerator thermal capacity ratio or temperature profiles internal to the wire, which are in any case now clearly identified as a separate similarity issue. It is significant that equation (18) embodies the characteristic Reynolds number and compactness ratio, $R_H/r$. The presence of the other two terms, $\lambda_h$ and $\alpha_x$, calls for three applications to check two heat exchangers and one regenerator. If the equation provides a valid criterion, it might be expected to return similar values between successful, high power-density designs, and, say, a successful small hot-air engine.

For the MP1002CA at rated conditions (Table 1), equation (18) has the numerical value 140. From data on General Motors' GPU3 tabulated in reference (**3**) but taking account of the fact that *rated* working fluid was $H_2$ (diatomic) at 69 bar $N_{SG} = 19.7E + 09$, $N_{MA}$ (based on $r$) = 5.6E-04 and $R_H/r = 0.0107$. For the regenerator $r_h/r = 1.9E\text{-}03$ and $\alpha_{xr} = 1.126E\text{-}03$. Equation (18) then has the value 110, which, given the differences in individual parameters, is promisingly close to the 140 for the MP1002CA. Exact correspondence would prove nothing, since the $N_T$ differ somewhat, and the difference contravenes dynamic similarity.

The Kyko hot-air engine has piston and displacer bores of 2.125 in, $r = 0.812$ in, a displacer length of 7.0 in and a regenerative gap of 0.0395 in. It runs loaded at about 350 r/min on air at atmospheric pressure. $T_{ref}$ is ambient and $T_e$ is not known, but is almost certainly less than for the other two engines. The resulting difference in $N_T$ technically invalidates comparison via equation (18), but, with this qualification, a numerical result will be seen to be worth achieving. Operating conditions give $N_{SG} = 0.952E + 09$, $N_{MA} = 3.8E\text{-}04$, $R_H/r = 0.0664$, $\lambda_r = 0.0243$ and $\alpha_{xr} = 0.00213$. With these figures equation (18) returns the numerical value 104. Against a background of orders-of-magnitude difference between individual respective parameter values for the three designs, the close correspondence between the final values supports use of equation (18) to evaluate gas circuit geometry in relation to operating conditions.

## 7 CONCLUSIONS

1. The appropriate choice of independent variable so simplifies ideal cycle analysis as to permit construction of a respectable fluid particle displacement diagram to scale and without algebraic manipulation.
2. Use of the diagram in conjunction with numerical values of characteristic dimensionless parameters gives $p$, $C_f$ and $N_{st}$ as a function of location and crank angle without the need for a computer.
3. A gas circuit parameter has been defined and shown to unify the thermodynamic design of the Philips MP1002CA, the General Motors GPU-3 and the Kyko engines.

## REFERENCES


1 **deBrey, H., Rinia, H.** and **van Weenen, F. L.** Fundamentals for the development of the Philips air engine. *Philips Tech. Rev.*, 1947, **9**(4), 97–124.

2 **Organ, A. J.** *Stirling engine thermodynamic design—without the computer*, 1991 (mRT, Cambridge).

3 **Organ, A. J.** *Thermodynamics and gas dynamics of the Stirling cycle machine*, 1992 (Cambridge University Press, Cambridge).

4 **Organ, A. J.** Intimate design of the Stirling engine gas circuit without the computer. *Proc. Instn Mech. Engrs, Part C*, 1991, **205**(C6), 421–430.

5 **Gedeon, D.** Personal communication to the author on the subject of reference (**4**), November 1991.

6 **Organ, A. J.** Fluid particle trajectories in Stirling cycle machines. *J. Mech. Engng Sci.*, 1978, **20**(1), 1–10.

7 **Organ, A. J.** A thumb-nail sketch of the gas processes in the Stirling cycle machine. *Proc. Instn Mech. Engrs, Part C*, 1992, **206**(C4), 239–248.

8 **Takase, C. N.** Otimisação do dempenho específico de motores Stirling (Optimization of the specific performance of Stirling engines). MSc dissertation, Instituto Tecnológico de Aeronáutica, São José dos Campos, Est. de São Paulo, Brazil, 1972.

9 **White, F. M.** *Fluid mechanics*, 1979 (McGraw-Hill Kogakusha, Tokyo).

10 **Organ, A. J.** Steady-flow $C_f$–$N_{re}$ correlations for the wire gauze regenerator inferred from linear wave analysis. Under review by IMechE for possible publication in *Proceedings Part C*, 1993.

11 **Creswick, F. A.** Thermal design of Stirling cycle machines. SAE Automotive Engineering Congress, Detroit, Michigan, 11–15 January 1965, paper 949C.

12 **Finkelstein, T.** Generalized thermodynamic analysis of Stirling engines. Proceedings of SAE Winter Annual Meeting, 1960, paper 118B.

13 **Organ, A. J.** Flow in the Stirling regenerator characterized in terms of complex admittance. Part 1: theoretical development. Under review by IMechE for publication in *Proceedings Part C*, 1993.

14 **Organ, A. J.** and **Rix, D. H.** Flow in the Stirling regenerator characterized in terms of complex admittance. Part 2: experimental investigation. Under review by IMechE for publication in *Proceedings Part C*, 1993.


## APPENDIX

**Characteristic dimensionless groups** (see Table 2)

1. The inventory of dimensionless groups applies to *kinematic* Stirling machines. The *principle* of dynamic similarity extends without reservation to other types, such as the free-piston/displacer, Ringbom, etc., and most of the present groups are applicable. However, additional groups are needed to characterize the other variants.
2. The inventory covers the case of *internal dynamic similarity*. This means that the internal surfaces of expansion and compression exchangers, and of the associated variable-volume spaces, are held at the rated temperature for all choices of the governing characteristic groups. The principle is eminently capable of extension to dynamic similarity of the transient heat flow from the heat source through the exchanger walls to the inner surface, and from the inner surface of the compression exchanger through the walls to the ultimate sink. Additional characteristic groups are needed to achieve this.
3. The reference length chosen for earlier definitions (**2–4**) was $R_H$, the characteristic hydraulic radius. $R_H$ is an important characteristic dimension of the Stirling machine gas circuit, but it is now considered that it is best employed as the *link* between drive kinematics and gas circuit by defining the group $R_H/r$, where $r$ is the crank radius or equivalent. The role of the reference linear dimension is now taken over by the crank radius, $r$. $R_H/r$ might be thought of as the 'compactness ratio'.

4. A group formerly (**2–4**) used, namely $N_H$, is now replaced by the thermal capacity ratio $N_{TCR}$. The substitution is on the strength of the more self-evident physical significance of $N_{TCR}$. As required by the principles of dynamic similarity, the total number of groups remains unchanged, $N_{TCR}$ being obtained by substitution of $N_F$ into $N_H$.
5. Regenerator scaling calls for a similarity of construction—square woven mesh to square woven mesh, filament-wound to filament-wound, etc.
6. All work and efficiency quantities are *indicated* values.
7. The validity of the proposed set of characteristic groups as criteria for the *internal* dynamic similarity of Stirling cycle machines rests on the fact that numerical values for each of the groups constitutes a necessary and sufficient set of data for an analysis and/or computer simulation of the cycle embodying gas circuit geometry, gas law, three differential conservation laws (mass, momentum and energy) for the gas and the general heat conduction equation for transients internal to the individual regenerator wire. Operation of any two gas circuits defined by the same numerical values of the parameter set have an identical computed indicated performance by definition. To this extent they are dynamically similar.

**Table 2** List of dimensionless variables through which may be specified *internal dynamic similarity* between respective gas circuits and operating conditions of two Stirling cycle machines

| Symbol | Definition | Physical significance |
|---|---|---|
| $\zeta$ | $W_{cycle}/(p_{ref} V_{ref})$ | Standard definition of normalized cycle work |
| $\eta$ | $W_{cycle}/Q_e$ | Standard definition of indicated thermal efficiency |
| $N_T$ | $T_e/T_{ref} = T_e/T_c$ | Characteristic temperature ratio |
| $\gamma$ | $c_p/c_v$ | Specific heat ratio. Strict dynamic similarity applies only between working fluids of the same $\gamma$ |
| $\kappa$ | $V_C/V_E$ | (Equivalent) swept volume ratio |
| $\alpha$ | | (Equivalent) volume phase angle |
| | If the simple harmonic approximation is unacceptable, exact equivalence between practical drive mechanisms may be specified in terms of dimensionless ratios of all lengths defining kinematics and piston diameters. | |
| $\mu_E$ | $V_E/V_{ref}$ | |
| $\mu_{dxe}$, $\mu_{de}$, etc. | $V_{dxe}/V_{ref}$, etc. | Ratios of dead volumes to reference volume |
| $\alpha_{xe}$, $\alpha_{xc}$ | $A_{xe}/A_{ref}$, etc. | Ratios of free-flow areas to reference area |
| | Specification of dead volume and free-flow area determines length in the case of the parallel exchanger. *Either* volumes *or* areas may be substituted by lengths if the alternative combination is preferred. | |
| $\lambda_{he}$, $\lambda_{hr}$ | $r_{he}/L_{ref}$, etc. | Normalized hydraulic radius |
| $\P_v$ | | Volumetric porosity of regenerator matrix |
| $n_{gauze}$ | | Number of gauzes in stacked screen regenerator. Linear wave analysis (**10**, **13**, **14**) has recently confirmed that two regenerators of stacked screen type are fully dynamically similar *only* if of the same weave, same porosity, $\P_v$, same $r_h/r$ *and of the same total number of screens.* Equivalent parameters are required of regenerators fabricated by other means, for example by filament winding |
| $N_{MA}$ | $n_s r/\sqrt{(RT_{ref})}$ | Characteristic Mach number. Two dynamically similar machines operating with the same numerical value of $N_{MA}$ have identical compressibility effects at all locations and for all crank angles |
| $N_{RE}$ | $N_{SG} N_{MA}^2$ | Characteristic Reynolds number. All other things being equal, two machines with the same numerical value of $N_{RE}$ have the same friction factor $C_f$ and the same Stanton/Prandtl product $N_{st}/N_{pr}^{2/3}$ at all locations and for all crank angles. Dimensionless temperature distribution $T/T_{ref}$ and dimensionless pressure drops $\Delta p/p$ (or $\Delta p/p_{ref}$) are therefore the same at all locations for all crank angles |
| $N_{SG}$ | $p_{ref}/(n_s \mu_{ref})$ | Characteristic Stirling number (cf. Sommerfeld number). Ratio of pressure effects to viscous effects |
| $N_{TCR}$ | $p_{ref}/(T_{ref} \rho_r c_r)$ | Characteristic thermal capacity ratio, equivalent for given $\gamma$ to $\rho c_p/(\rho_r c_r)$. Constancy of the numerical value of this group, together with that of $N_F$ (below), is the condition for equal (dimensionless) regenerator temperature swings |
| $N_F$ | $\alpha_r/(n_s r^2)$ | Characteristic Fourier number for the regenerator. All other things being equal, a common value of $N_F$ between two machines ensures identical profiles of (dimensionless) temperature inside the regenerator wires at all locations and for all values of (dimensionless) time, that is of crank angle |